PCCP

ROYAL SOCIETY OF CHEMISTRY

PAPER

View Article Online
View Journal | View Issue

Cite this: *Phys. Chem. Chem. Phys.*, 2023, **25**, 28428

Unveiling the intersystem crossing dynamics in N-annulated perylene bisimides†

Jeswin Sunny, ‡[a] Ebin Sebastian, ‡[a] Suvarna Sujilkumar, ‡[a] Frank Würthner, [b] Bernd Engels *[c] and Mahesh Hariharan *[a]

Received 14th August 2023,
Accepted 9th October 2023

DOI: 10.1039/d3cp03888b

rsc.li/pccp

The efficient population of the triplet excited states in heavy metal-free organic chromophores has been one of the long-standing research problems to molecular photochemists. The negligible spin–orbit coupling matrix elements in the purely organic chromophores and the large singlet–triplet energy gap (ΔE_{S-T}) pose a hurdle for ultrafast intersystem crossing (ISC). Herein we report the unprecedented population of triplet manifold in a series of nitrogen-annulated perylene bisimide chromophores (NPBI and Br-NPBI). NPBI is found to have a moderate fluorescence quantum yield (Φ_f = 68 ± 5%), whereas Br-NPBI showcased a low fluorescence quantum yield (Φ_f = 2.0 ± 0.6%) in toluene. The femtosecond transient absorption measurements of Br-NPBI revealed ultrafast ISC (k_{ISC} = 1.97 × 10^{10} s^{-1}) from the initially populated singlet excited state to the long-lived triplet excited states. The triplet quantum yields (Φ_T = 95.2 ± 4.6% for Br-NPBI, Φ_T = 18.7 ± 2.3% for NPBI) calculated from nanosecond transient absorption spectroscopy measurements showed the enhancement in triplet population upon bromine substitution. The quantum chemical calculations revealed the explicit role of nitrogen annulation in tuning the excited state energy levels to favor the ISC. The near degeneracy between the singlet and triplet excited states observed in NPBI and Br-NPBI (ΔE_{S-T} = −0.01 eV for NPBI, ΔE_{S-T} = 0.03 eV for Br-NPBI) facilitates the spin flipping in the molecules. Nitrogen annulation emerges as a design strategy to open up the ISC pathway and the rate of which can be further enhanced by the substitution of a heavier element.

Introduction

Intersystem crossing (ISC), a non-radiative transition involving spin flipping, is the quintessential process for populating the triplet manifold in chromophoric systems.[1,2] The efficient population and harvest of triplet excitons find diverse applications in organic light-emitting diodes,[3–5] organic photovoltaics,[6–9] photodynamic therapy,[10,11] photocatalysis,[12,13] *etc.* The long diffusion lengths of the triplet excitons have been exploited in optoelectronic devices to enhance the photocurrent as it increases the possibility of charge separation at donor–acceptor interfaces.[8] The generation of reactive singlet oxygen *via* triplet sensitization from chromophores finds applications in photodynamic therapy.[11,14] As a result, chromophores exhibiting efficient ISC are in great demand.

Perylene bisimides (PBIs) are a class of highly sought-after n-type organic semiconductor materials for optoelectronic applications owing to their excellent electron affinity and mobility.[15,16] The large molar absorption coefficient, high stability, easier tunability of electronic properties, *etc.*, are attractive features of PBIs.[16,17] A vital role in controlling the rate of ISC process in organic materials is played by spin–orbit coupling (SOC).[1,18] In addition to SOC, the reduction in the singlet–triplet energy gap is important for enhancing the rate of intersystem crossing.[2] Several strategies have been reported till date to generate triplet excitons, ranging from the conventional heavy atom effect,[19] vibronic coupling,[18,20] core twist,[21–23] multiexciton generating singlet fission,[24–28] and charge recombination.[29–35] Seminal works by Castellano and co-workers[36] and Würthner and co-workers[37,38] have shown that incorporating transition metals to rylene bisimides enhances SOC-driven ISC. The large nuclear charge associated with transition metals imparts large SOC, thereby enhancing the rate of ISC.[2] The cytotoxicity associated with chromophores encompassing heavy metals proposes the need for purely organic molecular materials exhibiting an enhanced triplet population. As an alternative strategy, non-metallic elements,

[a] *School of Chemistry, Indian Institute of Science Education and Research Thiruvananthapuram (IISER TVM), Vithura, Thiruvananthapuram, Kerala, 695551, India. E-mail: mahesh@iisertvm.ac.in*
[b] *Institut für Organische Chemie & Center for Nanosystems Chemistry, Universität Würzburg, Am Hubland, 97074 Würzburg, Germany*
[c] *Institut für Physikalische und Theoretische Chemie, Universität Würzburg, Emil-Fischer-Strasse 42, 97074 Würzburg, Germany*

† Electronic supplementary information (ESI) available: Adiabatic energies and plots, nsTA features, triplet and singlet oxygen quantum yield. See DOI: https://doi.org/10.1039/d3cp03888b

‡ These authors contributed equally.

including heavier halogens[39–42] and chalcogens[43–47] have been appended to chromophores to enhance the ISC rates. An unusual halogen bond-directed heavy atom effect was observed by Kim and co-workers in phosphorescent crystals of bromine-substituted aromatic carbonyls.[48]

The continuous efforts from our group in populating the triplet manifold have been fruitful in generating near unity triplet quantum yield in eight bromine atoms substituted PBI driven by the synergistic effect of core-twist and spin–orbit coupling.[49] Herein, we report the observation of an ultrafast triplet population in a single bromine atom substituted nitrogen-annulated PBI (Br-NPBI) chromophore. Nitrogen-annulated PBI (NPBI) is found to have a moderately large fluorescence quantum yield (Φ_f = 68 ± 5%). Upon single bromine substitution at the bay position of NPBI, the fluorescence quantum yield remarkably decreases, rendering ultrafast ISC in Br-NPBI (Φ_f = 2.0 ± 0.6%). On the contrary, the unsubstituted PBI and mono-brominated Br-PBI exhibits strong fluorescence (Φ_f ~ 100% for PBI and Φ_f = 97% for Br-PBI). The transient absorption measurements in the femtosecond and nano-second time regimes explicitly confirm the population of triplet excited states in Br-NPBI and NPBI. The quantum chemical calculations support the observation of triplet formation in Br-NPBI and NPBI, where efficient ISC occurs between the nearly degenerate S_1 and T_2 excited states (ΔE_{S-T} = −0.01 eV for NPBI, ΔE_{S-T} = 0.03 eV for Br-NPBI). The high singlet–triplet energy gap forbids the ISC pathway in PBI and Br-PBI. The present work sheds light on the research quest to achieve efficient triplet exciton formation in organic materials for advanced optoelectronic applications.

Experimental

Photophysical measurements

Steady-state and time-resolved optical measurements of the compounds were carried out in standard quartz cuvettes having path length of 1 cm for solutions in dried and distilled solvents. Electronic absorption spectra were recorded on Shimadzu UV-3600 UV-Vis-NIR, while emission and gated emission spectra were recorded on Horiba Jobin Yvon Fluorolog 3 spectrometer. The pulse width of the flash lamp for gated measurement is 3 μs.

Estimating triplet quantum yield (Φ_T)

To estimate the triplet quantum yield (Φ_T) of Br-NPBI/NPBI, the process of triplet energy transfer to β-carotene was used with $[Ru(bpy)_3]^{2+}$ as the reference (Φ_T ~ 1) as reported in the literature.[50–52] A known, equal volume of β-carotene in $CHCl_3$ was added to the optically matched solutions (0.1–0.2 absorbance at 532 nm) of $[Ru(bpy)_3]^{2+}$ in methanol and Br-NPBI/NPBI in toluene. The energy transfer from $[Ru(bpy)_3]^{2+}$ or Br-NPBI/NPBI populates the β-carotene triplet, which is monitored at 530 nm. The Φ_T values of the PBI derivatives were calculated according to the following equation where super-scripts "Sam" and "Ref" refers to the sample Br-NPBI/NPBI and reference $[Ru(bpy)_3]^{2+}$ respectively. k_{obs} is the pseudo-first-order rate constant for the growth of the β-carotene triplet, and k_0 is the rate constant for the decay of the donor triplets (in the absence of β-carotene) in solutions that contained $[Ru(bpy)_3]^{2+}$ or Br-NPBI/NPBI with same absorbance.

$$\Phi_T^{Sam} = \Phi_T^{Ref} \times \frac{\Delta A^{Sam}}{\Delta A^{Ref}} \times \frac{k_{obs}^{Sam}}{k_{obs}^{Sam} - k_0^{Sam}} \times \frac{k_{obs}^{Ref} - k_0^{Ref}}{k_{obs}^{Ref}}$$

Singlet oxygen ($^1O_2$) quantum yields (Φ_Δ)

The singlet oxygen quantum yield ($^1O_2$) measurements were carried out using Rose Bengal (RB) in methanol as a standard having a $^1O_2$ quantum yield of 0.80.[53,54] 1,3-Diphenylisobenzofuran (DPBF) in de-aerated dimethylformamide (DMF) solvent acts as the $^1O_2$ scavenger, having absorbance around 1.0. The Br-NPBI (photosensitizer), was added into the cuvette (OD ~ 0.2–0.3) containing DPBF. The cuvette was photo-irradiated using of 532 nm monochromatic light, and the absorption spectra was recorded in every 2 s interval. The slope of absorbance maxima of DPBF at 414 nm with irradiation time was plotted. Singlet oxygen quantum yield (Φ_Δ^{Sam}) was calculated according to a modified equation.

$$\Phi_\Delta^{Sam} = \Phi_\Delta^{Ref} \times \frac{k(Sam)}{k(Ref)} \times \frac{F(Ref)}{F(Samp)}$$

where k is the slope of the difference in the change in the absorbance of DPBF (at 414 nm) with irradiation time and F is the absorption correction factor, which is given by $F = 1–10^{OD}$ (OD at the irradiation wavelength).

Femtosecond transient absorption measurements

A Spectra-Physics Mai Tai SP mode-locked laser (800 nm, 86 MHz) was used as a seed for Spectra-Physics Spitfire Ace regenerative amplifier (1 kHz, 5.5 mJ). Using TOPAS, a portion of the amplified 800 nm output beam was converted into a 470 nm pump pulse. An 800 nm residual pulse passing through the ExciPro pump−probe spectrometer optical delay line (3.5 ns) was used in the generation of a white light continuum using calcium fluoride crystal. White light continuum passes through a beam splitter to produce the probe and the reference pulse. The femtosecond transient absorption spectra of the samples were recorded using a dual diode array detector, having a detection window and optical delay of 200 nm and 3.5 ns, respectively. Sample solutions were prepared in a 1.2 mm path length rotating cuvette. Determination of instrument response function (IRF) is essential for the accurate deconvolution of the spectra. IRF was determined by a two-photon absorption experiment using 10% benzene in a methanol solution and was found to be approximately 110 fs at 530 nm. Samples were excited at 470 nm with 100 fs pulses, and the use of a neutral density filter controlled the incident flux of the sample.

Nanosecond transient absorption measurements

Nano-second laser transient absorption experiments of the samples were carried out in an Applied Photophysics Model

LKS-60 laser kinetic spectrometer. Nitrogen-purged solution of samples were excited using the second harmonic (532 nm, pulse duration ~8 ns) of a Quanta Ray INDI-40–10 series pulsed Nd:YAG laser. Oxygen-purged experiments confirm the presence of the triplet excited state through nanosecond transient absorption studies.

Global analysis

Glotaran software is used for the global analysis of fsTA and nsTA data of the samples. The method evaluates the group velocity dispersion of the white light continuum and instrument response function (IRF), which allows accurate estimation of decay time constants and dispersion-compensated spectra. Global analysis of fsTA data carried out in a sequential model resulted in evolution-associated spectrum (EAS) with decay time constants.[55]

Computational details

The ground state geometries of the Br-NPBI, NPBI, Br-PBI, and PBI were optimized using density functional theory (DFT) at CAM-B3LYP56/def2-SVP level of theory. Singlet excited states were computed using the time-dependent DFT (TD-DFT).[56] Using the Tamm–Dancoff approximation (TDA) instead of TD-DFT the agreement to the experimental results deteriorates significantly (Table S6, ESI†). For triplet states, however, the Tamm–Dancoff approximation (TDA) were employed since it provides more reliable energies for such states.[57] For all calculations the range-separated CAM-B3LYP functional in combination with def2-SVP and aug-cc-pVDZ[58] basis sets were used. To obtain information about the shapes of the corresponding potential energy curves the S_1 as well as the T_2 equilibrium geometries were also determined. The spin–orbit coupling matrix elements between the spin singlet and triplet excited states were computed at the CAM-B3LYP/aug-cc-pVDZ levels of theory using the PySOC package.[59,60] All the quantum chemical calculations were carried out using Gaussian 16 package.[61]

Results and discussion

In this work, a series of perylene bisimide derivatives (PBI, Br-PBI, NPBI, and Br-NPBI) were synthesized and characterized following previously reported procedures (Fig. 1 and Scheme S1, ESI†).[62,63] The geometries of the derivatives in the ground state were optimized using DFT at CAM-B3LYP/def2-SVP levels of theory (Fig. S1, ESI†). Unsubstituted PBI exhibited a planar structure in the ground state, whereas optimized geometry of Br-PBI revealed that the substitution of bromine atom on the bay position of PBI imposed a core twist in the chromophore with a twist angle of 20.6°. The optimized geometry of NPBI showcased a planar scaffold with a bowed geometry. The 5-membered heterocyclic ring formed, with a carbon-nitrogen bond length of 1.40 Å, imposed the inward bend in the core. The substitution of the bromine atom in the bay position of NPBI resulted in a negligible twist in the core, resulting in planar Br-NPBI. The insignificant core twist in Br-NPBI resulted from the reduced steric repulsion between the bromine and hydrogen atoms in the bay position supported by bowed geometry of the molecule (Fig. S1, ESI†).

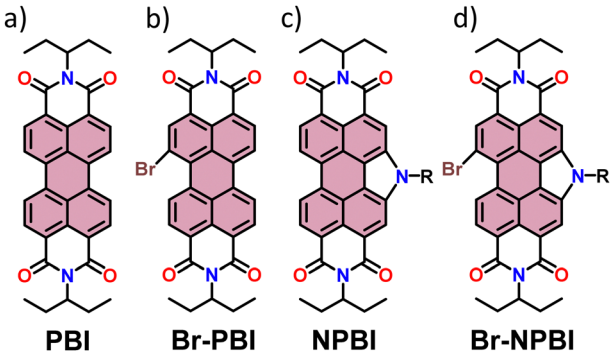

Fig. 1 Molecular structures of (a) PBI, (b) Br-PBI, (c) NPBI, and (d) Br-NPBI. *R* in the chemical structure denotes *n*-hexyl chain.

The steady-state optical measurements of PBI derivatives were performed in toluene at room temperature. The photophysical properties of PBI, Br-PBI, and NPBI, observed from the steady-state optical measurements, were consistent with the previous reports.[22,63] The UV-Vis absorption spectra of PBI, Br-PBI, NPBI, and Br-NPBI show distinct vibronic features as a result of the strong coupling between the vinyl stretching modes of the PBI core ($\upsilon_{C=C}$ ~ 1400 cm^{-1}), and the $S_0 \rightarrow S_1$ electronic transition (Fig. 2 and Fig. S2, ESI†). The UV-visible absorption spectrum of Br-NPBI showed two distinct absorption bands centered at 526 nm and 491 nm, corresponding to the 0-0, and 0-1 vibronic transitions, respectively. NPBI exhibited two distinct absorption bands at 527 nm and 492 nm

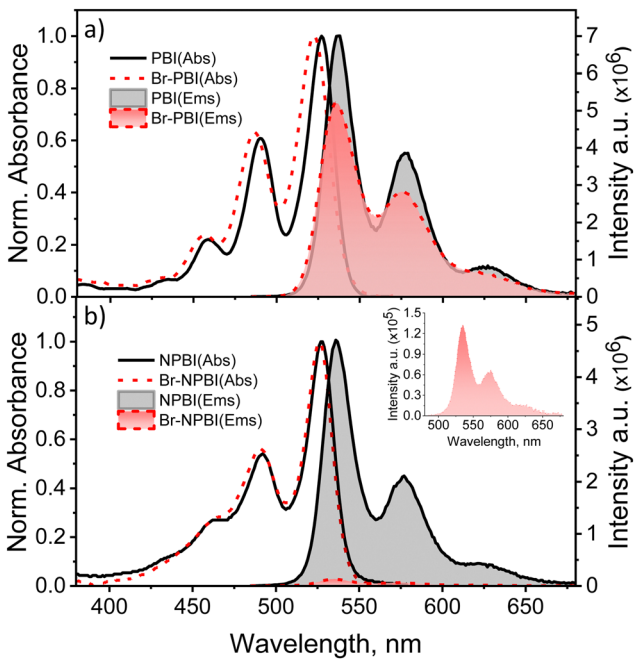

Fig. 2 Normalized UV-Vis absorption and fluorescence emission spectra of PBI and Br-PBI (top) and NPBI and Br-NPBI (bottom) in toluene. The enlarged fluorescence emission spectrum of Br-NPBI is shown in the inset.

Table 1 Photoexcited properties of PBI, Br-PBI, NPBI, and Br-NPBI. λ_{abs}; absorption maximum, λ_f; emission maximum

	λ_{abs} (nm eV^{-1})	λ_f (nm)	Φ_f (%)	Φ_T (%)
PBI	527/2.35	538	$\sim 100^a$	—
Br-PBI	522/2.38	535	97^a	—
NPBI	527/2.35	536	68 ± 5^a	18.7 ± 2.3
Br-NPBI	526/2.36	535	2.0 ± 0.6	95.2 ± 4.6

[a] Fluorescence quantum yield was obtained from previously published results[63,64]

corresponding to the 0-0, and 0-1 vibronic transitions, respectively. The absorption spectrum of Br-PBI showed three distinct vibronic bands at 522, 487, and 457 nm, whereas the unsubstituted PBI showcased vibronic bands centered at 527, 490, and 459 nm (Table 1).

The fluorescence emission spectra of Br-NPBI, NPBI, Br-PBI, and PBI revealed mirror images of the corresponding absorption spectra. Br-NPBI showed emission bands at 535 nm and 571 nm, whereas NPBI has emission bands centered at around 536 and 577 nm. The unsubstituted PBI has emission bands centered at 538, 577, and 627 nm, and Br-PBI has emission bands centered at 535, 575, and 628 nm (Fig. 2 and Fig. S3, ESI†). The fluorescence quantum yields (Φ_f) of the PBI derivatives were measured in toluene at room temperature. NPBI showed fluorescence quantum yield, $\Phi_f = 68 \pm 5\%$, compared to $\Phi_f \sim 100\%$ for PBI and $\Phi_f = 97\%$ for Br-PBI. Solvent-dependent fluorescence quantum yield measurements of Br-NPBI and NPBI have been carried out in acetone and acetonitrile solvents (Table S1, ESI†). Surprisingly, bromine substitution on NPBI reduced the fluorescence quantum yield to $2.0 \pm 0.6\%$ (Table 1). The observed reduction in the fluorescence quantum yield can be attributed to competitive non-radiative processes occurring from the S_1 state.

The heavy atom effect induced by bromine atom substitution is known to enhance the ISC rate.[49,64,65] However, a single bromine substitution on the PBI core has negligible effect on the triplet population.[22] The SOC induced by the single bromine atom on PBI is inadequate for the enhancement of the ISC rate, as evident from the fluorescence quantum yield (Table 1). The reduced fluorescence in NPBI and the remarkably low fluorescence in its mono-brominated derivative, Br-NPBI, suggests the possibility of an enhanced triplet population in the molecules. Vauthey and coworkers reported ultrafast ISC in bromine and nitrogen-substituted naphthalene bisimide chromophore.[42] The rate of the ISC can be theoretically determined using the Fermi golden rule where the rate constant of ISC depends on the SOC.[66]

To understand the competitive decay pathways from the singlet excited state, femtosecond transient absorption (fsTA) measurements were carried out in toluene at room temperature. The fsTA spectra of NPBI were adapted from ref. 63. The fsTA spectra of NPBI (Fig. 3a) after photoexcitation at 470 nm

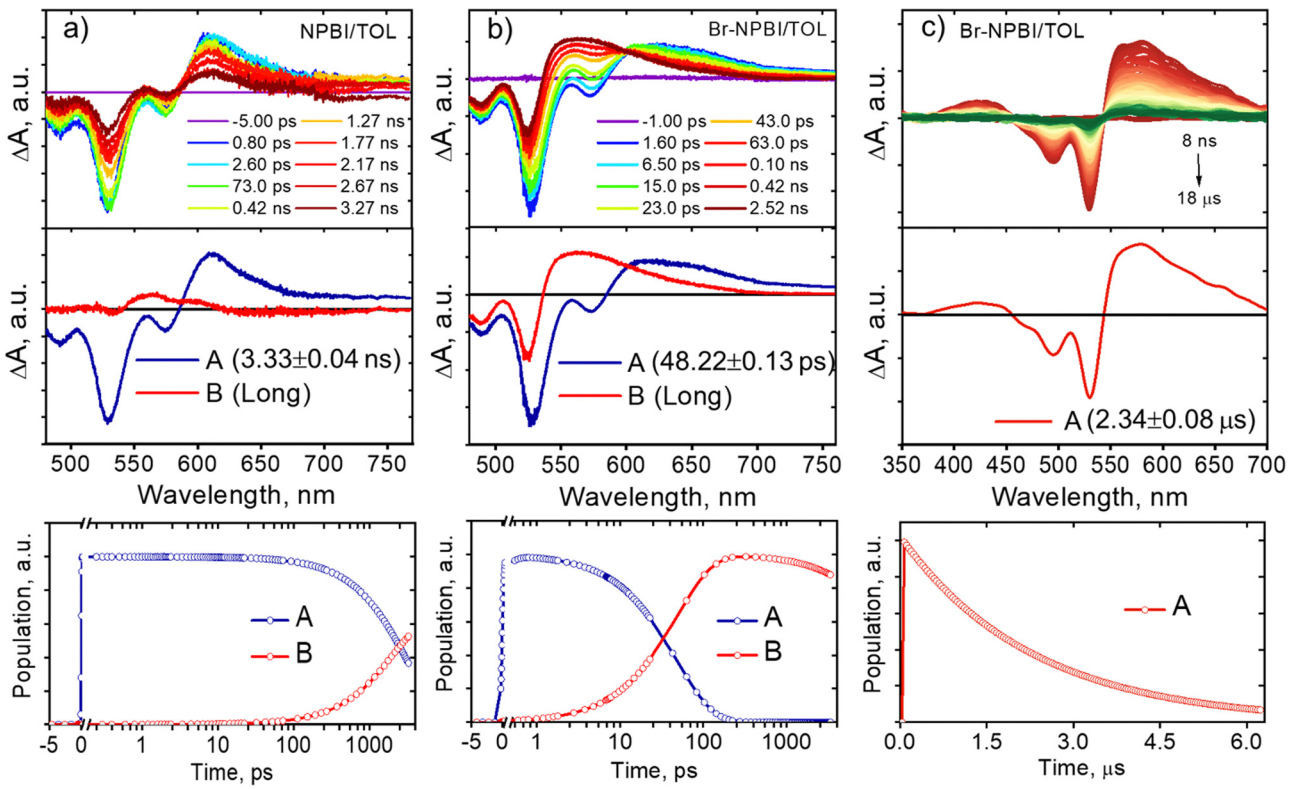

Fig. 3 (Top) Femtosecond transient absorption spectra of (a) NPBI (adapted from ref. 63) and (b) Br-NPBI in toluene. Nanosecond transient absorption spectra of (c) Br-NPBI in toluene. (Middle) EAS reconstructed from global analysis. (Bottom) The relative population profiles of the excited states fitted using kinetic model.

show negative ground state bleach (GSB) ranging from 480 nm to 557 nm. The band at 530 nm have contributions from both GSB and stimulated emission (SE). The band at 574 nm corresponds to higher vibronic bands of SE. The positive excited state absorption (ESA) lies in the region from 587 nm to 655 nm. In the initial delay times, NPBI shows ESA spectral features centered at 609 nm. As the delay time increases, the spectral signal decays with the slow evolution of a weak ESA feature centered at 570 nm. To elucidate the kinetics of the spectral evolution, a global analysis of the fsTA spectra was performed. The evolution-associated spectrum (EAS) of NPBI, was acquired by fitting using a two-component sequential kinetic model (A → B → GS). The two components can be attributed to two distinct excited state transitions, $S_1 \rightarrow S_n$ and $T_1 \rightarrow T_n$. The initially populated singlet state spectral signature decays with the gradual evolution of spectral features corresponding to the triplet manifold. The ESA of the newly formed transient species centered at 570 nm can be attributed to the $T_1 \rightarrow T_n$ transition. The fsTA spectra of Br-NPBI (Fig. 3b) after photoexcitation at 470 nm showed similar ESA and GSB compared to NPBI in the initial delay time. The positive spectral signature ranging from 613 nm to 627 nm attributed to the initially populated singlet state decay in ultrafast timescale ($\tau_{A\rightarrow B}$ = 48.22 ± 0.13 ps), leading to the population of a new state with ESA centered at 570 nm. The decay of the newly formed species is not complete within the experimental time window. The de-convolution of the fsTA spectra was carried out through global analysis, extracting the EAS. The EAS of Br-NPBI was fitted into two components using a sequential kinetic model (A → B → GS). The first component (A) of the EAS is attributed to the absorption from the first singlet excited state to higher singlet states. The spectral signature associated with this transition decays in ultrafast timescale with (k_{ISC}) with the evolution of the second EAS component. The second component (B) can be attributed to the absorption from the first triplet excited state to higher triplet states.

Nanosecond transient absorption (nsTA) measurements of NPBI and Br-NPBI in toluene at room temperature were carried out to understand the dynamics of the excited state in the longer delay times. Photoexcitation at 532 nm of nitrogen-purged solution of NPBI resulted in a positive peak centered at around 570 nm and a negative peak corresponding to the ground state bleach ranging from 470 nm to 545 nm (Fig. S4, ESI†). The positive spectral signature at 570 nm was quenched upon oxygen-purging of the NPBI solution, confirming the triplet population (Fig. S5, ESI†). The decay time constant of the triplet excited state of NPBI was found to be 1.42 ± 0.23 μs (Fig. S4, ESI†) in the degassed solution with a quantum yield (Φ_T) of 18.7 ± 2.3% (Fig. S6, ESI†). nsTA measurements of nitrogen-purged Br-NPBI (Fig. 3c) solution in toluene showed an intense positive peak centered at around 570 nm after photoexcitation at 532 nm. The nsTA spectra showed ground state bleach in the region from 460 nm to 540 nm. The formation of a triplet excited state in Br-NPBI is confirmed by the depletion in the spectral peak intensity at 570 nm after purging the solution with oxygen (Fig. S7, ESI†). The decay time constant of the long-lived triplet excited state was found to be τ_T = 2.34 ± 0.08 μs. The triplet quantum yield of Br-NPBI in toluene was estimated to be Φ_T = 95.2 ± 4.6% using a triplet–triplet energy transfer mechanism (Fig. S8, ESI†). The singlet oxygen quantum yield (Φ_Δ) of Br-NPBI is estimated using Rose Bengal (RB) as a standard in methanol.[54] Singlet oxygen quantum yield for Br-NPBI was found to be 86.0% using Rose Bengal as a standard (Fig. S9, ESI†). nsTA measurements of Br-PBI were carried out in toluene at room temperature. Photoexcitation at 532 nm of nitrogen-purged solution of Br-PBI showed no significant positive absorption, indicating the negligible intersystem crossing in the Br-PBI (Fig. S10, ESI†).

The gated emission measurements of Br-NPBI and NPBI were carried out exciting at 470 nm and 472 nm, respectively, at 77 K in toluene. For Br-NPBI (delay time of 0.05 ms, slit width 1.5 mm) the gated emission band was observed at 599 nm with a lifetime of 11.8 μs (Fig. S11, ESI†). Gated measurements of NPBI at 77 K exhibited a band at 597 nm (delay time of 0.05 ms, slit width 1.5 mm) with a lifetime of 7.5 μs (Fig. S12, ESI†).

To rationalize the role of bromine and nitrogen substitution on PBI molecule in enhancing the ISC rate, we performed quantum chemical calculations. The computed excitation energies with respect to the S_0 ground state in its equilibrium geometry $R(S_0)$ using the range-separated CAM-B3LYP functional[67] in combination with aug-cc-pVDZ basis sets[58] are summarized in Table 2. The corresponding data using the smaller def2-SVP basis sets[68,69] are given in Tables S2–S5 (ESI†). The data are also plotted in Fig. S14 and S15 (ESI†) for a better overview.

The absorption spectra of the compounds (Fig. 2) show a three-band vibrational progression so that the most intense band given in Table 1 must be assigned to the transition between the lowest vibrational states of S_0 and the S_1 (0-0 transition). The other bands then result from excitations to higher vibrational states of the S_1 (Fig. 4). The small difference between λ_{abs} and λ_f also indicates 0-0 transitions for absorption and emission. For all molecules, they differ only by about 0.05 eV, which most likely results from solvent effects. To model the vibrational progression and the exact energetic location of the 0-0 band, calculations that take into account the influence of nuclear motion are necessary, as we have recently shown in a benchmark.[70] However, this benchmark also proved that adiabatic excitation energies (see Fig. 4 and Fig. S13, ESI†) approximate the 0-0 excitation energy to within about 0.1 eV, while simple vertical energies overestimate 0-0 transition energies by up to 0.3 eV.

Table 2 shows similar effects for the molecules examined in this paper. For PBI, the vertical energy of 2.70 eV calculated with CAMB3LYP/aug-cc-pVDZ (Table 2: $E(S_1)$ at $R(S_0)$) overestimates the experimentally measured 0-0 transition (Table 1: 527 nm = 2.35 eV) by about 0.35 eV. In contrast, the adiabatic excitation energy of 2.45 eV (Table 2: $E(S_1)$ at $R(S_1)$) deviates by only 0.1 eV, which is similar to the inaccuracy found in our benchmark for adiabatic energies. If one uses the smaller def2-SVP basis (Tables S2–S5, ESI†), the deviations from the experimental data increase by about 0.1 eV. For Br-PBI, the picture is

Table 2 Energies of the PBI, Br-PBI, NPBI, and Br-NPBI were computed at S_0, S_1, T_1, and T_2 states using CAM-B3LYP/aug-cc-pVDZ level of theory

	Energy relative to the ground state energy at $R(S_0)$ in eV															
	PBI				Br-PBI				NPBI				Br-NPBI			
Geometry	S_0	S_1	T_1	T_2	S_0	S_1	T_1	T_2	S_0	S_1	T_1	T_2	S_0	S_1	T_1	T_2
$R(S_0)$	0	2.70	1.64	2.93	0	2.72	1.69	2.92	0	2.82	1.82	2.66	0.0	2.83	1.86	2.64
$R(S_1)$	0.18	2.45	1.37	2.92	0.21	2.49	1.39	2.91	0.15	2.64	1.60	2.65	0.15	2.66	1.63	2.63
$R(T_2)$	0.29	2.61	1.46	2.88	0.29	2.60	1.47	2.84	0.11	2.74	1.71	2.54	0.11	2.74	1.74	2.53

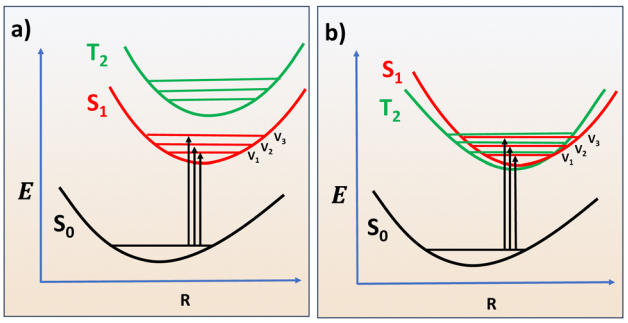

Fig. 4 Schematic representation of potential energy surfaces of S_0, S_1, and T_2 of (a) Br-PBI/PBI and (b) Br-NPBI/NPBI demonstrating the possibility of ISC.

identical. For NPBI and Br-NPBI, however, the adiabatic energies deviate by about 0.3 eV from the experimental 0-0 transitions listed in Table 1. We attribute this somewhat stronger deviation to a more complex electronic structure, possibly resulting from the influence of the strain resulting from the ring formation.

However, more precise calculations are not necessary because the main difference between PBI/Br-PBI (high fluorescence quantum yield) and NPBI/Br-NPBI (low fluorescence quantum yield) results from the changes in the energetic sequence of S_1 and T_2 (Table 2 and Fig. S14, ESI†), which are clearly indicated by our calculations. For all four molecules, the T_1 is well below the S_1 (>1.0 eV), so an S_1–T_1 singlet–triplet transition as a reason for decreasing (fluorescence quantum yields) can be ruled out. For PBI and Br-PBI, the T_2 for $R(S_1)$ is about 0.5 eV above the S_1, so that an S_1–T_2 transition can also be excluded. For NPBI and Br-NPBI, however, the picture changes completely. For both molecules, our calculations predict that the S_1 and the T_2 are nearly degenerate (Table 2 and Fig. 4) inducing very efficient S_1–T_2 transitions even for the small spin–orbit couplings calculated for NPBI or Br-NPBI (Table S7, ESI†). The greatly reduced fluorescence yield of Br-NPBI compared to NPBI could result from larger SOC couplings, but this is not supported by the calculations (Table S7, ESI†) which predict a similar size of the couplings. Hence, we attribute this experimental finding to subtle different energetic positions of both states for Br-NPBI and NPBI being outside of the accuracy of the employed theoretical approach. The situation is sketched in Fig. 4. For PBI and Br-PBI, the T_2 lies above the S_1, so no ISC can happen. For NPBI and Br-NPBI, the T_2 lies below the S_1 for $R(S_0)$ but both are nearly energy degenerate so that after the excitation, an efficient S_1–T_2 ISC can take place.

Conclusions

In summary, we report the unprecedented triplet population in NPBI and Br-NPBI facilitated by a reduced singlet–triplet energy gap. The moderate and low fluorescence quantum yields were observed for NPBI and Br-NPBI, respectively. The concerted interplay of nitrogen annulation and single bromine substitution fosters efficient intersystem crossing in Br-NPBI with ISC rate, $k_{ISC} = 1.97 \times 10^{10}\ s^{-1}$ as observed from the fsTA measurements. The triplet quantum yield is enhanced from $\Phi_T = 18.7 \pm 2.3\%$ in NPBI to $\Phi_T = 95.2 \pm 4.6\%$ for Br-NPBI which could be rationalized as the effect of bromine substitution. The nsTA spectroscopy revealed the long decay times for the triplet states in NPBI and Br-NPBI. Theoretical investigations suggest the significant role of nitrogen annulation in diminishing the singlet–triplet energy gap in NPBI and Br-NPBI. The low ΔE_{S-T} value activates the ISC pathway in both NPBI and Br-NPBI, whereas the additional effect of bromine in Br-NPBI enhances the ISC rates to the ultrafast regime. The current work sheds light on the novel design strategies for triplet exciton generation in molecular materials, which have profound implications for developing organic light-emitting diodes and organic solar cells.

Conflicts of interest

There are no conflicts to declare.

Acknowledgements

M. H. acknowledges the Department of Science and Technology (DST) Nanomission [DST/NM/TUE/EE-01/2019] for the support of this work. We thank the support for the high-performance computing time at the Padmanabha cluster at IISER TVM. E. S. and S. S. acknowledge UGC and IISER TVM, respectively, for financial assistance.

Notes and references

1 N. J. Turro, V. Ramamurthy and J. C. Scaiano, *Modern Molecular Photochemistry of Organic Molecules*, University Science Books, 2010.

2 M. Hariharan, D. Sasikumar, A. T. John and J. Sunny, Access to the triplet excited states of organic chromophores, *Chem. Soc. Rev.*, 2020, **49**, 6122.
3 J. Lee, H. F. Chen, T. Batagoda, C. Coburn, P. I. Djurovich, M. E. Thompson and S. R. Forrest, Deep blue phosphorescent organic light-emitting diodes with very high brightness and efficiency, *Nat. Mater.*, 2016, **15**, 92–98.
4 C. Adachi, M. A. Baldo, M. E. Thompson and S. R. Forrest, Nearly 100% internal phosphorescence efficiency in an organic light-emitting device, *J. Appl. Phys.*, 2001, **90**, 5048–5051.
5 Z. An, C. Zheng, Y. Tao, R. Chen, H. Shi, T. Chen, Z. Wang, H. Li, R. Deng, X. Liu and W. Huang, Stabilizing triplet excited states for ultralong organic phosphorescence, *Nat. Mater.*, 2015, **14**, 685–690.
6 M. Einzinger, T. Wu, J. F. Kompalla, H. L. Smith, C. F. Perkinson, L. Nienhaus, S. Wieghold, D. N. Congreve, A. Kahn, M. G. Bawendi and M. A. Baldo, Sensitization of silicon by singlet exciton fission in tetracene, *Nature*, 2019, **571**, 90–94.
7 A. Rao and R. H. Friend, Harnessing singlet exciton fission to break the Shockley–Queisser limit, *Nat. Rev. Mater.*, 2017, **2**, 17063.
8 J. Lee, P. Jadhav, P. D. Reusswig, S. R. Yost, N. J. Thompson, D. N. Congreve, E. Hontz, T. Van Voorhis and M. A. Baldo, Singlet Exciton Fission Photovoltaics, *Acc. Chem. Res.*, 2013, **46**, 1300–1311.
9 W.-Y. Wong and C.-L. Ho, Organometallic Photovoltaics: A New and Versatile Approach for Harvesting Solar Energy Using Conjugated Polymetallaynes, *Acc. Chem. Res.*, 2010, **43**, 1246–1256.
10 V. N. Nguyen, Y. Yan, J. Zhao and J. Yoon, Heavy-Atom-Free Photosensitizers: From Molecular Design to Applications in the Photodynamic Therapy of Cancer, *Acc. Chem. Res.*, 2021, **54**, 207–220.
11 T. C. Pham, V.-N. Nguyen, Y. Choi, S. Lee and J. Yoon, Recent Strategies to Develop Innovative Photosensitizers for Enhanced Photodynamic Therapy, *Chem. Rev.*, 2021, **121**, 13454–13619.
12 L. Schmid, F. Glaser, R. Schaer and O. S. Wenger, High Triplet Energy Iridium(III) Isocyanoborato Complex for Photochemical Upconversion, Photoredox and Energy Transfer Catalysis, *J. Am. Chem. Soc.*, 2022, **144**, 963–976.
13 F. Strieth-Kalthoff, M. J. James, M. Teders, L. Pitzer and F. Glorius, Energy transfer catalysis mediated by visible light: principles, applications, directions, *Chem. Soc. Rev.*, 2018, **47**, 7190–7202.
14 L. A. Ortiz-Rodríguez, S. J. Hoehn, A. Loredo, L. Wang, H. Xiao and C. E. Crespo-Hernández, Electronic Relaxation Pathways in Heavy-Atom-Free Photosensitizers Absorbing Near-Infrared Radiation and Exhibiting High Yields of Singlet Oxygen Generation, *J. Am. Chem. Soc.*, 2021, **143**, 2676–2681.
15 A. Nowak-Król, K. Shoyama, M. Stolte and F. Würthner, Naphthalene and perylene diimides – better alternatives to fullerenes for organic electronics?, *Chem. Commun.*, 2018, **54**, 13763–13772.
16 X. Zhan, A. Facchetti, S. Barlow, T. J. Marks, M. A. Ratner, M. R. Wasielewski and S. R. Marder, Rylene and Related Diimides for Organic Electronics, *Adv. Mater.*, 2011, **23**, 268–284.
17 C. Li and H. Wonneberger, Perylene Imides for Organic Photovoltaics: Yesterday, Today, and Tomorrow, *Adv. Mater.*, 2012, **24**, 613–636.
18 T. J. Penfold, E. Gindensperger, C. Daniel and C. M. Marian, Spin-Vibronic Mechanism for Intersystem Crossing, *Chem. Rev.*, 2018, **118**, 6975–7025.
19 D. S. McClure, Triplet–Singlet Transitions in Organic Molecules. Lifetime Measurements of the Triplet State, *J. Chem. Phys.*, 1949, **17**, 905–913.
20 R. A. Vogt and C. E. Crespo-Hernández, Conformational Control in the Population of the Triplet State and Photoreactivity of Nitronaphthalene Derivatives, *J. Phys. Chem. A*, 2013, **117**, 14100–14108.
21 P. Malakar, V. Borin, A. Bedi, I. Schapiro, O. Gidron and S. Ruhman, The impact of twisting on the intersystem crossing in acenes: an experimental and computational study, *Phys. Chem. Chem. Phys.*, 2022, **24**, 2357–2362.
22 K. Nagarajan, A. R. Mallia, K. Muraleedharan and M. Hariharan, Enhanced intersystem crossing in core-twisted aromatics, *Chem. Sci.*, 2017, **8**, 1776–1782.
23 C. A. M. Salla, G. Farias, M. Rouzières, P. Dechambenoit, F. Durola, H. Bock, B. de Souza and I. H. Bechtold, Persistent Solid-State Phosphorescence and Delayed Fluorescence at Room Temperature by a Twisted Hydrocarbon, *Angew. Chem., Int. Ed.*, 2019, **58**, 6982–6986.
24 M. B. Smith and J. Michl, Singlet Fission, *Chem. Rev.*, 2010, **110**, 6891–6936.
25 T. Ullrich, D. Munz and D. M. Guldi, Unconventional singlet fission materials, *Chem. Soc. Rev.*, 2021, **50**, 3485–3518.
26 K. Miyata, F. S. Conrad-Burton, F. L. Geyer and X.-Y. Zhu, Triplet Pair States in Singlet Fission, *Chem. Rev.*, 2019, **119**, 4261–4292.
27 J. Xia, S. N. Sanders, W. Cheng, J. Z. Low, J. Liu, L. M. Campos and T. Sun, Singlet Fission: Progress and Prospects in Solar Cells, *Adv. Mater.*, 2017, **29**, 1601652.
28 A. Mandal, M. Chen, E. D. Foszcz, J. D. Schultz, N. M. Kearns, R. M. Young, M. T. Zanni and M. R. Wasielewski, Two-Dimensional Electronic Spectroscopy Reveals Excitation Energy-Dependent State Mixing during Singlet Fission in a Terrylenediimide Dimer, *J. Am. Chem. Soc.*, 2018, **140**, 17907–17914.
29 M. L. Williams, I. Schlesinger, R. M. Jacobberger and M. R. Wasielewski, Mechanism of Ultrafast Triplet Exciton Formation in Single Cocrystals of π-Stacked Electron Donors and Acceptors, *J. Am. Chem. Soc.*, 2022, **144**, 18607–18618.
30 Z. E. X. Dance, S. M. Mickley, T. M. Wilson, A. B. Ricks, A. M. Scott, M. A. Ratner and M. R. Wasielewski, Intersystem Crossing Mediated by Photoinduced Intramolecular Charge Transfer: Julolidine−Anthracene Molecules with Perpendicular π Systems, *J. Phys. Chem. A*, 2008, **112**, 4194–4201.
31 M. Lv, X. Lu, Y. Jiang, M. E. Sandoval-Salinas, D. Casanova, H. Sun, Z. Sun, J. Xu, Y. Yang and J. Chen, Near-Unity Triplet

Generation Promoted via Spiro-Conjugation, *Angew. Chem., Int. Ed.*, 2022, **61**, e202113190.

32 X. Chen, A. A. Sukhanov, M. Taddei, B. Dick, J. Zhao, V. K. Voronkova and M. Di, Donato, Charge Separation/Recombination, Intersystem Crossing, and Unusually Slow Intramolecular Triplet–Triplet Energy Transfer in Naphthalenediimide–Anthracene Compact Energy Donor–Acceptor Dyads, *J. Phys. Chem. Lett.*, 2022, **13**, 8740–8748.

33 X. Xiao, I. Kurganskii, P. Maity, J. Zhao, X. Jiang, O. F. Mohammed and M. Fedin, A long-lived charge-separated state of spiro compact electron donor–acceptor dyads based on rhodamine and naphthalenediimide chromophores, *Chem. Sci.*, 2022, **13**, 13426–13441.

34 X. Wang, L. Martínez-Fernández, Y. Zhang, K. Zhang, R. Improta, B. Kohler, J. Xu and J. Chen, Solvent-Dependent Stabilization of a Charge Transfer State is the Key to Ultrafast Triplet State Formation in an Epigenetic DNA Nucleoside, *Chem. – Eur. J.*, 2021, **27**, 10932–10940.

35 Z. Wang, L. Ma, H. Zhao, Y. Wan, X.-F. Zhang, Y. Li, Z. Kuang and A. Xia, Spin–orbit charge-transfer intersystem crossing in heavy-atom-free orthogonal covalent boron-dipyrromethene heterodimers, *Phys. Chem. Chem. Phys.*, 2023, **25**, 24386–24394.

36 E. O. Danilov, A. A. Rachford, S. Goeb and F. N. Castellano, Evolution of the triplet excited state in Pt II perylenediimides, *J. Phys. Chem. A*, 2009, **113**, 5763–5768.

37 M. J. Sun, O. Anhalt, M. B. Sárosi, M. Stolte and F. Würthner, Activating Organic Phosphorescence via Heavy Metal–π Interaction Induced Intersystem Crossing, *Adv. Mater.*, 2022, **34**, 2207331.

38 M. Schulze, A. Steffen and F. Würthner, Near-IR phosphorescent ruthenium(II) and iridium(III) perylene bisimide metal complexes, *Angew. Chem., Int. Ed.*, 2015, **54**, 1570–1573.

39 G. Farias, C. A. M. Salla, M. Aydemir, L. Sturm, P. Dechambenoit, F. Durola, B. de Souza, H. Bock, A. P. Monkman and I. H. Bechtold, Halogenation of a twisted non-polar π-system as a tool to modulate phosphorescence at room temperature, *Chem. Sci.*, 2021, **12**, 15116–15127.

40 E. Pomarico, P. Pospíšil, M. E. F. Bouduban, J. Vestfrid, Z. Gross, S. Záliš, M. Chergui and A. Vlček, Photophysical Heavy-Atom Effect in Iodinated Metallocorroles: Spin–Orbit Coupling and Density of States, *J. Phys. Chem. A*, 2018, **122**, 7256–7266.

41 J. Vestfrid, M. Botoshansky, J. H. Palmer, A. C. Durrell, H. B. Gray and Z. Gross, Iodinated Aluminum(III) Corroles with Long-Lived Triplet Excited States, *J. Am. Chem. Soc.*, 2011, **133**, 12899–12901.

42 O. Yushchenko, G. Licari, S. Mosquera-Vazquez, N. Sakai, S. Matile and E. Vauthey, Ultrafast Intersystem-Crossing Dynamics and Breakdown of the Kasha–Vavilov's Rule of Naphthalenediimides, *J. Phys. Chem. Lett.*, 2015, **6**, 2096–2100.

43 J. Sivanarayanan, E. Sebastian, K. Vinod and M. Hariharan, Ultrafast Intersystem Crossing in Selenium-Annulated Perylene Bisimide, *J. Phys. Chem. C*, 2022, **2022**, 126–13319.

44 P. Mentzel, M. Holzapfel, A. Schmiedel, I. Krummenacher, H. Braunschweig, A. Wodyński, M. Kaupp, F. Würthner and C. Lambert, Excited states and spin–orbit coupling in chalcogen substituted perylene diimides and their radical anions, *Phys. Chem. Chem. Phys.*, 2022, **24**, 26254–26268.

45 R. D. Pensack, Y. Song, T. M. McCormick, A. A. Jahnke, J. Hollinger, D. S. Seferos and G. D. Scholes, Evidence for the Rapid Conversion of Primary Photoexcitations to Triplet States in Seleno- and Telluro- Analogues of Poly(3-hexylthiophene), *J. Phys. Chem. B*, 2014, **118**, 2589–2597.

46 F. Sadiq, Z. Wang, Y. Hou, J. Zhao, A. Elmali, D. Escudero and A. Karatay, Thienyl/phenyl bay-substituted perylenebisimides: Intersystem crossing and application as heavy atom-free triplet photosensitizers, *Dyes Pigm.*, 2021, **184**, 108708.

47 S. Mai, M. Pollum, L. Martínez-Fernández, N. Dunn, P. Marquetand, I. Corral, C. E. Crespo-Hernández and L. González, The origin of efficient triplet state population in sulfur-substituted nucleobases, *Nat. Commun.*, 2016, **7**, 13077.

48 O. Bolton, K. Lee, H.-J. Kim, K. Y. Lin and J. Kim, Activating efficient phosphorescence from purely organic materials by crystal design, *Nat. Chem.*, 2011, **3**, 205–210.

49 A. Mohan, E. Sebastian, M. Gudem and M. Hariharan, Near-Quantitative Triplet State Population via Ultrafast Intersystem Crossing in Perbromoperylenediimide, *J. Phys. Chem. B*, 2023, **2020**, 37.

50 S. K. Rajagopal, K. Nagaraj, S. Deb, V. Bhat, D. Sasikumar, E. Sebastian and M. Hariharan, Extending the scope of the carbonyl facilitated triplet excited state towards visible light excitation, *Phys. Chem. Chem. Phys.*, 2018, **20**, 19120–19128.

51 W. E. Ford and P. V. Kamat, Photochemistry of 3,4,9,10-perylenetetracarboxylic dianhydride dyes. 3. Singlet and triplet excited-state properties of the bis(2,5-di-tert-butylphenyl)imide derivative, *J. Phys. Chem.*, 1987, **91**, 6373–6380.

52 V. Karunakaran, D. D. Prabhu and S. Das, Optical Investigation of Self-Aggregation of a Tetrazole-Substituted Diphenylacetylene Derivative: Steady and Excited State Dynamics in Solid and Solution State, *J. Phys. Chem. C*, 2013, **117**, 9404–9415.

53 A. A. Buglak, A. Charisiadis, A. Sheehan, C. J. Kingsbury, M. O. Senge and M. A. Filatov, Quantitative Structure–Property Relationship Modelling for the Prediction of Singlet Oxygen Generation by Heavy-Atom-Free BODIPY Photosensitizers, *Chem. – Eur. J.*, 2021, **27**, 9934–9947.

54 L. Huang, Z. Li, Y. Zhao, Y. Zhang, S. Wu, J. Zhao and G. Han, Ultralow-Power Near Infrared Lamp Light Operable Targeted Organic Nanoparticle Photodynamic Therapy, *J. Am. Chem. Soc.*, 2016, **138**, 14586–14591.

55 I. H. M. van Stokkum, D. S. Larsen and R. van Grondelle, Global and target analysis of time-resolved spectra, *Biochim. Biophys. Acta, Bioenerg.*, 2004, **1657**, 82–104.

56 C. Adamo and D. Jacquemin, The calculations of excited-state properties with Time-Dependent Density Functional Theory, *Chem. Soc. Rev.*, 2013, **42**, 845–856.

57 C. Brückner and B. Engels, Benchmarking singlet and triplet excitation energies of molecular semiconductors for singlet fission: tuning the amount of HF exchange and adjusting local correlation to obtain accurate functionals for singlet–triplet gaps, *Chem. Phys.*, 2017, **482**, 319–338.

58 D. E. Woon and T. H. Dunning, Gaussian basis sets for use in correlated molecular calculations. III. The atoms aluminum through argon, *J. Chem. Phys*, 1993, **98**, 1358–1371.

59 X. Gao, S. Bai, D. Fazzi, T. Niehaus, M. Barbatti and W. Thiel, Evaluation of Spin–Orbit Couplings with Linear-Response Time-Dependent Density Functional Methods, *J. Chem. Theory Comput.*, 2017, **13**, 515–524.

60 R. Ahmed and A. K. Manna, Origins of Molecular-Twist-Triggered Intersystem Crossing in Functional Perylenediimides: Singlet–Triplet Gap versus Spin–Orbit Coupling, *J. Phys. Chem. A*, 2022, **126**, 6594–6603.

61 M. J. Frisch, G. W. Trucks, H. B. Schlegel, G. E. Scuseria, M. A. Robb, J. R. Cheeseman, G. Scalmani, V. Barone, G. A. Petersson, H. Nakatsuji, X. Li, M. Caricato, A. V. Marenich, J. Bloino, B. G. Janesko, R. Gomperts, B. Mennucci, H. P. Hratchian, J. V. Ortiz, A. F. Izmaylov, J. L. Sonnenberg, D. Williams-Young, F. Ding, F. Lipparini, F. Egidi, J. Goings, B. Peng, A. Petrone, T. Henderson, D. Ranasinghe, V. G. Zakrzewski, J. Gao, N. Rega, G. Zheng, W. Liang, M. Hada, M. Ehara, K. Toyota, R. Fukuda, J. Hasegawa, M. Ishida, T. Nakajima, Y. Honda, O. Kitao, H. Nakai, T. Vreven, K. Throssell, J. A. Montgomery, Jr., J. E. Peralta, F. Ogliaro, M. J. Bearpark, J. J. Heyd, E. N. Brothers, K. N. Kudin, V. N. Staroverov, T. A. Keith, R. Kobayashi, J. Normand, K. Raghavachari, A. P. Rendell, J. C. Burant, S. S. Iyengar, J. Tomasi, M. Cossi, J. M. Millam, M. Klene, C. Adamo, R. Cammi, J. W. Ochterski, R. L. Martin, K. Morokuma, O. Farkas, J. B. Foresman and D. J. Fox, *Gaussian 16, Revision C.01*, Gaussian, Inc., Wallingford CT, 2016.

62 A. D. Hendsbee, J.-P. Sun, W. K. Law, H. Yan, I. G. Hill, D. M. Spasyuk and G. C. Welch, Synthesis, Self-Assembly, and Solar Cell Performance of N-Annulated Perylene Diimide Non-Fullerene Acceptors, *Chem. Mater.*, 2016, **28**, 7098–7109.

63 E. Sebastian, J. Sunny and M. Hariharan, Excimer evolution hampers symmetry-broken charge-separated states, *Chem. Sci.*, 2022, **13**, 10824–10835.

64 K. Nagarajan, A. R. Mallia, V. S. Reddy and M. Hariharan, Access to Triplet Excited State in Core-Twisted Perylenediimide, *J. Phys. Chem. C*, 2016, **120**, 8443–8450.

65 S. Sarkar, H. P. Hendrickson, D. Lee, F. DeVine, J. Jung, E. Geva, J. Kim and B. D. Dunietz, Phosphorescence in Bromobenzaldehyde Can Be Enhanced through Intramolecular Heavy Atom Effect, *J. Phys. Chem. C*, 2017, **121**, 3771–3777.

66 C. M. Marian, Understanding and Controlling Intersystem Crossing in Molecules, *Annu. Rev. Phys. Chem.*, 2021, **72**, 617–640.

67 T. Yanai, D. P. Tew and N. C. Handy, A new hybrid exchange–correlation functional using the Coulomb-attenuating method (CAM-B3LYP), *Chem. Phys. Lett.*, 2004, **393**, 51–57.

68 F. Weigend and R. Ahlrichs, Balanced basis sets of split valence, triple zeta valence and quadruple zeta valence quality for H to Rn: design and assessment of accuracy, *Phys. Chem. Chem. Phys.*, 2005, **7**, 3297.

69 A. Schäfer, H. Horn and R. Ahlrichs, Fully optimized contracted Gaussian basis sets for atoms Li to Kr, *J. Chem. Phys.*, 1992, **97**, 2571–2577.

70 M. Deutsch, S. Wirsing, D. Kaiser, R. F. Fink, P. Tegeder and B. Engels, Geometry relaxation-mediated localization and delocalization of excitons in organic semiconductors: a quantum chemical study, *J. Chem. Phys.*, 2020, **153**, 224104.

